Decoupling of Confused Complex in Oxidation of 3,3',5,5'-Tetramethylbenzidine Enhancing Reliability of Chromogenic Bioassay

Caixia Zhu, Hong Yang, Xuwen Cao, Qing Hong, Yuan Xu, Kaiyuan Wang, Yanfei Shen*, Songqin Liu, Yuanjian Zhang*

Jiangsu Engineering Laboratory of Smart Carbon-Rich Materials and Devices, Jiangsu Province Hi-Tech Key Laboratory for Bio-Medical Research, School of Chemistry and Chemical Engineering, Medical School, Southeast University, Nanjing 21189, China. Email: Yanfei.Shen@seu.edu.cn (Y.S.); Yuanjian.Zhang@seu.edu.cn (Y.Z.)

Abstract

Pathway regulation of chemical reactions is an important means of precision chemistry. As an extremely important chromogenic substrate, 3,3',5,5'-tetramethylbenzidine (TMB) generally undertakes one-electron oxidation, but the reaction product (TMB_{ox1}), a confused complex, is unstable, which significantly hampers the practical applications, such as clinic enzyme-linked immunosorbent assay (ELISA). Herein, we report that sodium dodecyl sulfate (SDS)-based micelles could promote the direct two-electron oxidation pathway of TMB into more stable TMB_{ox2}. Different to the common processes of one-electron TMB oxidation by homogeneous peroxidase (POD) or other emerging heterogeneous nanocatalysts, the confused complex consisted of TMB and TMB_{ox1} was successfully decoupled by SDS micelles via spatial isolation and electrostatic effect. As a proof-of-concept application, glucose oxidase and SDS micelles were cascaded for glucose detection, and the selective two-electron oxidation of TMB endowed enhanced reliability and broader detection range of glucose chromogenic bioassays without any conventional strong acid termination.

Keywords: surfactant assemblies, TMB, reliability, glucose biosensors

Introduction

Chemistry has always been changing throughout time toward precision, particularly in recent years.[1] Precise regulation of chemical reaction processes helps to realize precise and controllable chemical synthesis with high selectivity and efficiency.[2] As a typical substrate and chromogenic probe, 3,3',5,5'-tetramethylbenzidine (TMB) features particular interest, due to its low toxicity and high sensitivity of response.[3-5] And horseradish peroxidase (HRP) has been widely used in immunochemistry due to its high catalytic efficiency and specificity under mild reaction conditions.[6-8] Along this line, HRP-H_2O_2-TMB has become the standard chromogenic system in the clinic enzyme-linked immunosorbent assay (ELISA), which generally detects the absorbance of the one-electron oxidation product of TMB (TMB_{ox1}).[9-11] Notably, TMB_{ox1} is essentially a blue charge-transfer complex, consisting of the parent diamine (TMB) and the two-electron oxidation product of diimine (TMB_{ox2}) in rapid equilibrium with a radical cation (Fig. 1a).[12] After free TMB is completely oxidized in bulk solution, the blue TMB_{ox1} would inevitably undergo one more electron oxidation into the yellow product (TMB_{ox2}). In this way, the absorbance measurement of blue TMB_{ox1} catalyzed by HRP is time dependent and unreliable in practical applications.[13-14] To address this problem, a terminator, typically a strong acid, is generally required,[15-17] but which is corrosive and would cause critical safety hazards in bioassay. Therefore, selective catalytic oxidation of TMB via a direct two-electron pathway is highly envisioned, preferably using artificial enzymes for further considering risks of denaturation, laborious purification and high costs of natural enzymes.

Since the discovery of Fe_3O_4 nanoparticles with intrinsic peroxidase (POD)-like activity in 2007, many nanomaterial-based artificial enzymes, termed nanozymes, have been reported.[18-20] Due to low cost, easy availability, and high stability against biodegradation, nanozymes have attracted increasing attention in a wide range of fields, such as biosensors, immunoassays, and cancer therapy.[21-24] Nonetheless, the oxidation product of TMB catalyzed by conventional POD-like nanozymes also follows the order of the blue TMB_{ox1} and later the yellow TMB_{ox2}. Notably, surfactants assemblies have also been intensively explored as the simplest enzyme mimics, which overcomes poor reactant solubility and promotes product formation by interacting substrates through hydrogen bonding, van der Waals forces, or hydrophobic interactions.[25-28] Interestingly, TMB is hydrophobic, while the oxidation products of TMB are hydrophilic and

positively charged.[14, 29-32] Considering the heterogeneity and local environment of surfactants in aqueous solution, we reason that a spatial separation of TMB and its oxidation products would occur, thus decoupling the confused complexation and leading to a selective two-electron oxidation reaction pathway of TMB. Rather than free diffusion, it is highly reminiscent of biological metabolon that regulates specific metabolic pathways in a confined space by passing intermediate product from one enzyme to the next. In this sense, surfactant assemblies in solution would not only accelerate the reaction rate but also control the reaction pathway, which is superior than nanozymes and natural HRP in bulk solution for chromogenic bioassay; but to the best of our knowledge, it has not been reported.

Here, we reported a selective two-electron oxidation of TMB using sodium dodecyl sulfate (SDS)-based micelles. Mechanism studies revealed that the SDS micelles played crucial roles in decoupling of confused complex not only by spatial isolation, but also via electrostatic isolation. As a result, the production of TMB_{ox2} was highly selective, fast, and stable, overcoming the long-term challenge of TMB_{ox1} that continuously changes with H_2O_2 catalyzed by natural HRP. Further cascading with glucose oxidase (GOD), as a proof-of-concept application, glucose was more reliably measured even in a broader range of time, using SDS-micelles-based H_2O_2-TMB chromogenic systems.

Results and discussion

Two-electron oxidation of TMB with SDS micelles. As a common surfactant, SDS has been successfully used as a promoter in many organic reactions because its micellar structures can dissolve water-insoluble organic compounds.[33] Inspired by this fact, SDS micelles were applied as a proof-of-concept to verify the feasibility of improving the reaction rate and controlling reaction pathway here in the dehydrogenation of TMB. As the most widely used chromogenic substrate for HRP, TMB can be oxidized to colored products through both one-electron and two-electron pathways. The one-electron oxidation product of TMB is denoted as TMB_{ox1}, which is blue (λ= 370 nm, 652 nm). It consists of a diamine/diimine charge-transfer complex and a radical cation ($TMB^{\bullet+}$) that are inter-transferable. The two-electron oxidation product of TMB only includes diimine, which is yellow (λ= 450 nm).[12] Figure 1a shows the equations for the oxidation of TMB to produce two colored products and their corresponding photographs. Interestingly, as shown in Figure 1b and Figure S1, when TMB (0.1 mM), H_2O_2 (100 mM), and SDS (10 mM) solutions were mixed in 1 mL of 0.1 M HAc-NaAc buffer solution (pH 3.5), an absorbance at 450 nm was observed immediately, while the other two controls not. It evidently demonstrated that the two-electron oxidation product of TMB, i.e., yellow TMB_{ox2}, was produced with H_2O_2, under the promotion of SDS micelles. TMB oxidation rate was calculated using the absorbance of TMB_{ox2} as a function of time. It was found that the steady-state kinetics for the SDS-involved reaction followed the typical Michaelis-Menten model, reminiscent of natural enzyme-driven reactions (Figure 1c, d).

To validate the products of the oxidation reaction, the substrate and oxidation products of TMB in the solution were explored using high-resolution electrospray ionization mass spectrometry (ESI-MS, Figure 1e, bottom panel). Prior to oxidation, a fragment of TMB ([M + H]) was observed at m/z 241.1706. As expected, the fragment downshifted to 239.0278 after oxidation. It demonstrated the dehydrogenation of the two $-NH_2$ moieties on TMB and the oxidation of TMB into TMB_{ox2}. The high-performance liquid chromatography (HPLC) chromatogram (Figure S2) also showed that the product of TMB in the presence of SDS micelles was TMB_{ox2}, similar to the yellow product obtained from HRP oxidation under extended reaction time. These results suggested that the SDS micelles accelerate the two-electron oxidation of TMB with H_2O_2.

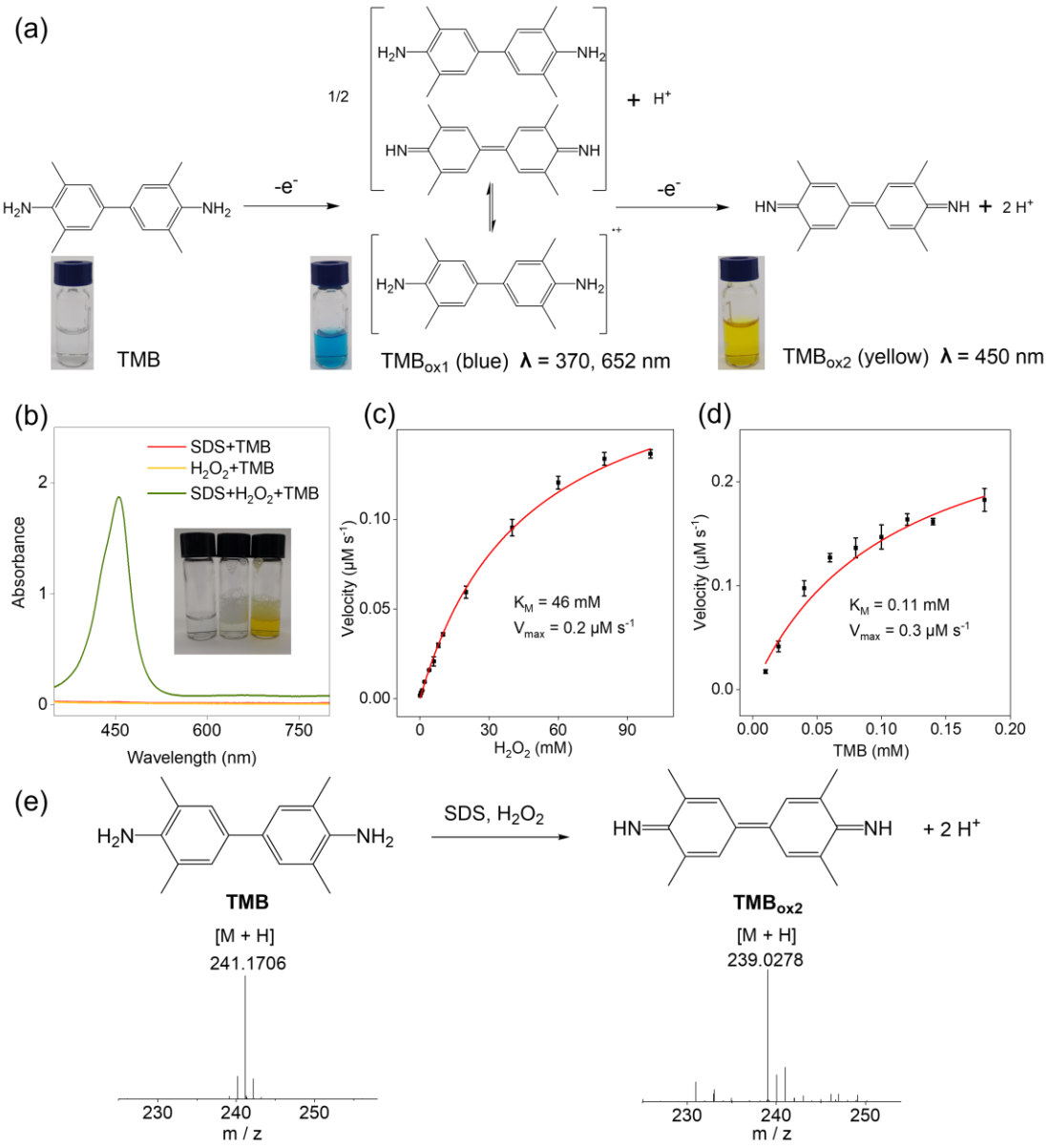

Figure 1. TMB oxidation in SDS micellar solution. (a) Reaction scheme and photographs for TMB oxidation catalyzed by HRP. (b) UV-vis absorption spectra of TMB (0.1 mM) after oxidation with SDS micelles in buffer solution containing 0.1 M H_2O_2. Typical Michaelis-Menten curves of SDS micelles with different concentration of (c) TMB ([H_2O_2]: 0.1 M) or (d) H_2O_2 ([TMB]: 0.1 mM) as substrate. (e) Reaction pathway of TMB oxidation in the presence of SDS micelles, as evidenced by the ESI-MS spectra of TMB and TMB_{ox2}. Buffer solution: 0.1 M HAc-NaAc. [SDS]: 10 mM.

Role of ROS on two-electron oxidation of TMB with SDS micelles. To understand the selective reaction pathway of TMB oxidation in the presence of the SDS micelles, possible intermediate radical species, such as free reactive oxygen species (ROS), were

explored using the scavenger trapping technique. UV-vis kinetic experiments were performed using isopropyl alcohol (IPA), 2,2,6,6-tetramethylpiperidine (TEMP), and superoxide dismutase (SOD) as scavengers for hydroxyl radicals, singlet oxygen, and superoxide radicals, respectively (Figure 2a). It was observed that the oxidation rate of TMB decreased dramatically after exclusively adding IPA, confirming that hydroxyl radicals were the primary radical intermediates in the oxidation reaction.[34] Moreover, the oxidation products increased with the amount of hydroxyl radicals, which positively correlated with the H_2O_2 concentration in the solution (Figure S3 and S4). Electron spin resonance (ESR) spectra were obtained to further confirm the type of ROS. As shown in Figure 2b, using 5,5-dimethyl-1-pyrroline N-oxide (DMPO) as the spin-trapping agent, distinct 4-fold characteristic peaks of hydroxyl radical-DMPO adducts with a signal intensity of 1:2:2:1 were observed both before and after adding SDS. The ESR spectra shown in Figure S5 further demonstrated that there were no signals for the superoxide radical and singlet oxygen-trapping agent adducts. These results again confirmed that hydroxyl radicals were the primary radical intermediates in the reaction process. However, it should be noted that the ESR signal intensities of the hydroxyl radicals in H_2O_2 buffer solutions remained unchanged before and after SDS addition (Figure 2b and c). This indicated that the hydroxyl radicals originated from the self-decomposition of H_2O_2, and the addition of SDS micelles did not increase the efficiency of hydroxyl radical production. Therefore, the mechanism of SDS micelles in the selective oxidation pathway of TMB did not follow the conventional pathway of activating H_2O_2 to form free or bounded ROS like HRP and typical nanozymes, such as Fe_3O_4 and Fe-N-C SACs.[35-36]

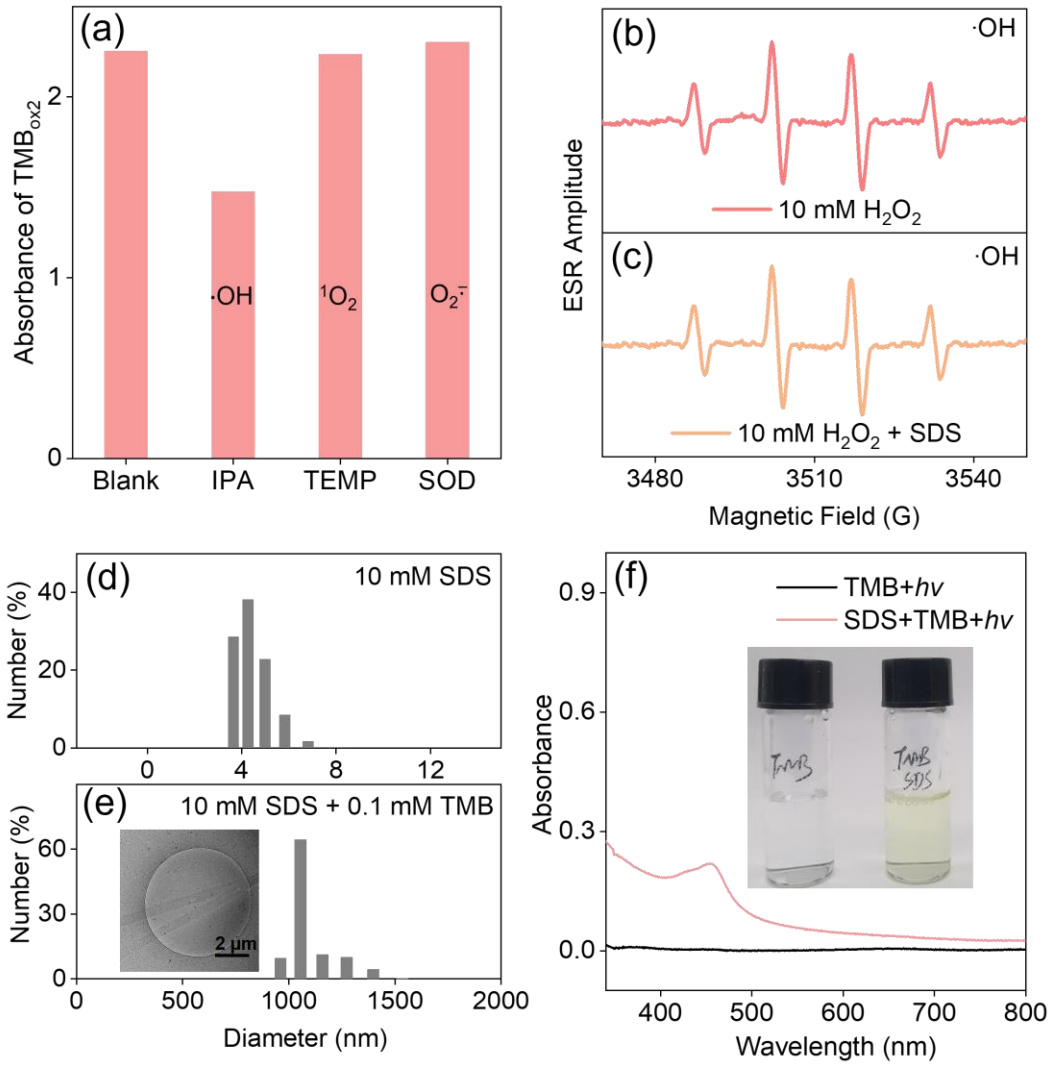

Figure 2. Intermediates in selective two-electron oxidation of TMB with SDS micelles. (a) Effects of ROS scavengers on the oxidation efficiencies of TMB with SDS micelles based on typical absorption at 450 nm (TMB_{ox2}). ESR spectra of the spin adduct of the hydroxyl radical generated by H_2O_2 (b) before and (c) after addition of SDS. DLS size distributions of SDS micelles before (d) and after (e) TMB addition. Inset: Cryo-TEM image of SDS micelles after the addition of TMB. (f) UV-vis absorption spectra of TMB after irradiation with visible light ($\lambda \geq 400$ nm) in aqueous solution with or without the addition of SDS micelles. Inset shows the photos. [SDS]: 10 mM.

Role of SDS micellar structure on two-electron oxidation of TMB. In general, the micellar microenvironment can change the state of the substrate or transition state, thereby affecting the reaction progress.[28, 37-38] As such, the interactions between SDS

micelles and substrate TMB in bimolecular reactions were investigated. The sizes of the particles in SDS micelles before and after TMB addition were measured by dynamic light scattering (DLS). As shown in Figure 2d, the micelle size in the pure SDS solution was approximately 4 nm, which was consistent with previous reports.[39-40] However, the micelle size increased dramatically to approximately 1000 nm after adding TMB (Figure 2e). In principle, when SDS is dissolved in water, there is a high degree of electrostatic repulsion between the head clusters in the micelles owing to the negative charge of the anion head clusters. This led to a sizeable effective head cluster area and a high micelle core curvature, resulting in the formation of spherical micelles. At concentrations much higher than the critical micelle concentration (CMC) or with additives, the micelles would undergo a morphological transformation into a cylindrical structure with a 100-1000 nm length.[40-41] The transformation is caused by reducing the effective area of the head cluster or by reducing the electrostatic repulsion. The transformation has been demonstrated experimentally and by all-atom molecular dynamics simulation studies of micelle front aggregation.[40, 42]

To determine the specific structure of the micelles in the mixed TMB and SDS systems, cryo-TEM imaging was performed, which showed a cylindrical form (Figure 2e, inset). These results further confirmed that the addition of TMB caused morphological changes in the micelles. It was mainly due to the hydrophobic interaction that drives TMB into the hydrophobic cavity of SDS micelles. Moreover, from a kinetic point of view, such confined space would improve the local concentration of reactants and accelerate the oxidation reaction rate, i.e., making TMB be in an "activated" state. To confirm this assumption, the TMB oxidation in aqueous solution with and without SDS micelles was explored under light irradiation (100 mW/cm^2, $\lambda \geq 400$ nm) that would photochemically produce trace amount of free ROS. Interestingly, the two-electron dehydrogenation of TMB was evidently observed with SDS micelles, while that of the control buffer solution not (Figure 2f), indicating their critical role in promote the reaction rate even when the concentration of oxidants was low. Therefore, in contrast to activating H_2O_2 oxidant via the common free ROS route or bound oxygen-atom transfer pathway for natural HRP and most peroxidase-like nanozymes, SDS micelles unusually accelerated the oxidative dehydrogenation process by activating TMB substrate.

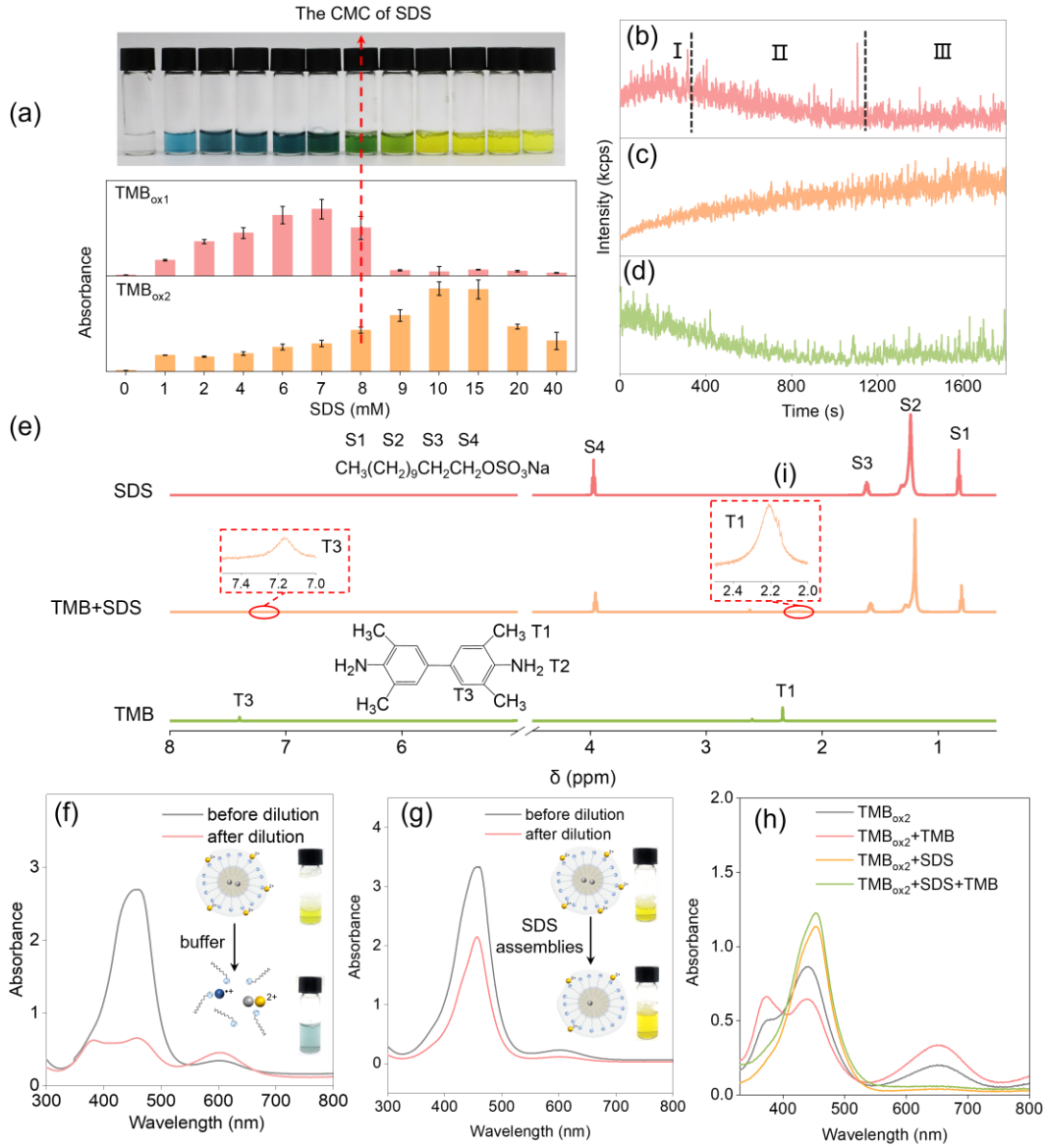

Figure 3. Spatial isolation of TMB two-electron oxidation product by SDS micelles. (a) Photographs and UV-vis absorbance at 600 nm (TMB_{ox1}) and 450 nm (TMB_{ox2}) of aqueous solutions containing TMB (0.1 mM) and SDS at different concentrations. (b) Time dependent scattered intensity of mixed solution containing 10 mM SDS, 0.05 mM TMB and 100 mM H_2O_2, or mixed solution containing 10 mM SDS and 0.05 mM TMB (c) before and (d) after addition of 100 mM H_2O_2. Scattering angle: 90°. (c) ^1H NMR spectra of SDS, TMB+SDS, and TMB in D_2O. UV-vis absorption spectra of TMB_{ox2} obtained by 10 mM SDS assemblies with 100 mM H_2O_2 before and after dilution using a buffer solution (d) and SDS assemblies (e). (f) UV-vis absorption spectra of TMB_{ox2} after the introduction of various substances.

The influence of different concentrations of SDS on the reaction pathway of TMB

oxidation was studied. As shown in Figure 3a, with an increase in SDS concentration, the color of the oxidation products gradually changed from blue (one-electron oxidation product) to yellow (two-electron oxidation product). This indicated that with an increase in SDS concentration, the oxidation products gradually changed from TMB_{ox1} to TMB_{ox2}. The product transition appeared at the critical micellar concertation (CMC) of SDS (ca. 8 mM), indicating the formation of SDS micelles played an essential role in altering the reaction pathway of TMB oxidation. The detailed UV-vis spectra also confirmed the transformation of the products (Figure S6). In addition, at concentrations much higher than the CMC of SDS (e.g., >15 mM) lower TMB_{ox2} conversion efficiencies were observed (Figure 3a). This was presumably due to the formation of a more "compact" structure of assemblies when the surfactant concentration constantly increased.[43-45] In this case, the diffusion of the H_2O_2 oxidant into the micellar inner cavities would be depressed, thus reduce the chance of collisions between reactants.[44] Therefore, the SDS concentration approaching CMC need optimization for the highly selective two-electron oxidation pathway for TMB.

Moreover, TMB encapsulating and product stabilization by the micellar structure was found to have a maximum capacity. As shown in Figure S7a, TMB (0.05 mM), H_2O_2 (100 mM), and SDS (10 mM) were added to the reaction solution, and the reaction products were only TMB_{ox2} from the beginning to the end of the reaction. It was supposed that when the TMB concentration was as low as 0.05 mM, the substrate TMB could be all encapsulated in the hydrophobic cavity. Due to electrostatic interactions, TMB_{ox2} would adsorb on the negatively charged outer surface. The substrate TMB and product TMB^{2+} thus cannot interact to form the electron transfer complex (TMB-TMB^{2+}). In this case, TMB_{ox2} was the only product. Interestingly, when the TMB concentration increased to 0.1 mM, the product at the beginning of the reaction was TMB_{ox2} (Figure S7b). However, as the time increased, the absorbance increase of TMB_{ox2} gradually slowed down, and the absorption peak of TMB_{ox1} began to appear. This trend became more significant when the TMB concentration increased to 0.2 mM (Figure S7c). It indicated that there was a maximum amount of TMB_{ox2} stabilized by micellar nanozymes (10 mM). Similarly, the amount of TMB that can be encapsulated by the hydrophobic pocket had an up limit. In addition, as shown in Figure S8, when

the micelle concentration increased to 20 mM, the amount of TMB_{ox2} that could be stabilized by micellar nanozymes also increased. The product TMB_{ox1} did not appear until the TMB concentration reached 0.2 mM. It showed that the up limit of TMB_{ox2} stabilization relied on the micelle concentration. Therefore, an optimization of SDS and TMB concentration was essential to achieve a highly selective two-electron oxidation pathway of TMB.

Spatial and electrostatic decoupling of confused complex by SDS micelles. To understand reactants and products migration in SDS micelles, in-situ dynamic light scattering experiments for TMB oxidation were performed.[46] Figure 3b shows the evolution of the scattering intensity with time. No significant change was observed in the scattering intensity of SDS micelle alone, indicative of a quasi-stable system (Figure S9). Interestingly, the profile of the scattered intensity with time for the solution containing SDS, TMB and H_2O_2 can be divided into three stages (Figure 3b). In stage I, the scattered intensity gradually increased, indicating that the encapsulation process for TMB by SDS micelles was dominant. The inner hydrophobic structure of SDS micelles drove TMB into the hydrophobic cavity, making the micellar structure became progressively larger. To further verify this process, ^{1}H NMR spectroscopy was explored.[47-48] As shown in Figure 3e, the chemical shifts of TMB varied from 7.40 and 2.34 ppm to 7.17 and 2.22 ppm after adding SDS micellar solution, respectively. The change in TMB chemical shift confirmed the interaction between SDS and TMB. In stage II, a gradual decrease in the scattering intensity was observed, indicating the oxidation of TMB and the departure of the oxidation product from the SDS micelles. Due to the positive electrical and hydrophilic nature of the oxidation products,[29, 31] the oxidation products would move to the outer surface of the micelles that was hydrophilic and negatively charged properties. To verify this assumption, the zeta potential of the mixed solution of SDS micelles (10 mM) and TMB (0.05 mM) was determined to be -61.55 ± 1.14 mV, while the zeta potential of the solution changed to -37.43 ± 1.65 mV after the addition of H_2O_2 (100 mM). The deceased of the negative zeta potential supported the absorption of positive two-electron TMB oxidation product on the out

surface of SDS micelles. Then, in this stage, the micelles gradually become smaller. In stage III, the dispersion intensity tended to be constant, indicating that the reaction was complete. As controls, the scattered intensity changes of SDS micelles solution, after only TMB was added, were monitored. As shown in Figure 3c, the scattered intensity gradually increased and eventually stabilized. It indicated that the micellar encapsulation of the substrate made the micellar particles increasingly larger, corresponding to stage I of Figure 3b. Afterwards, H_2O_2 was added to the above stabilized micellar solution. It was found that the oxidation of TMB leads to the decrease of light intensity (Figure 3d), corresponding to stage II of Figure 3b. Thus, these results again confirmed the encapsulation of the TMB substrate and the release of the TMB_{ox2} product during the oxidation reaction.

Interestingly, when the surfactant concentration reached the CMC, the two-electron oxidation product TMB_{ox2} was the only product. To get insights of this phenomenon, in the first set of experiments, an equal volume of buffer solution was used to dilute the TMB solution after the two-electron oxidation, i.e., TMB_{ox2} solution. As shown in Figure 3f, compared with the UV-vis absorption spectra of the original product solution, the absorbance of TMB_{ox2} (450 nm) decreased sharply, whereas that of TMB_{ox1} (600 nm), the one-electron product, increased. It was assumed that the dilution destroyed the original micelle structure that stabilized TMB_{ox2}. Such phenomenon of micelle disruption was verified by comparing the Tyndall effect before and after the dilution of the SDS micelle solution (Figure S10). Along this line, the TMB molecules encapsulated in the micelles should be released and complex with TMB_{ox2}, regenerating blue TMB_{ox1} (Figure 3f). As a control, an equal volume of SDS micelle (10 mM) solution was added to TMB_{ox2} solution. In this case, the SDS concentration of the solution remained unchanged. As shown in Figure 3g, a decrease in the absorbance of TMB_{ox2} (450 nm) was observed; however, there was no increase in the absorbance of TMB_{ox1} (600 nm). Consistently, the color of the solution did not turn blue but only became lighter. Therefore, we speculated that the stabilizing effect of SDS on TMB_{ox2} was mainly related to the micellar structure of SDS.

To further confirm the above hypothesis, more control experiments were performed (Figure 3h). The pure TMB_{ox2} solution was obtained by irradiating the TMB solution with full light. The method avoided the possible interferences in the solution. When TMB is added to the solution of TMB_{ox2}, TMB_{ox2} and TMB would undergo a redox reaction to form TMB_{ox1} (red line). However, when TMB was introduced into the solution of TMB_{ox2} after adding SDS micelles, no blue product was formed (green line), even though the amount of TMB added gradually increased (Figure S11). This indicates that TMB_{ox2} can be stabilized as long as micelles are present and sufficient in the solution. In addition, the important role of electrostatic interaction for TMB oxidation was explored by a series of control experiments using surfactants with different changes (see Figure S13-15 and more details in supporting information). In these regards, we speculated that the stabilization effect of SDS on TMB_{ox2} was mainly related to the stern layer of micelles, where TMB_{ox2} was stabilized and not easy to react again.

Density functional theory studies of electrostatic decoupling of confused complex by SDS micelles. To gain further insight into the decoupling effect of the confused complexation between TMB and TMB_{ox2} in the stern layer of micelles, density functional theory (DFT) calculations were performed on charge-transfer complex composed with TMB. In general, TMB_{ox2} (diamine) in an acidic open solution would be positively charged by binding two protons and denoted as TMB_{ox2}^{2+}. After stabilized on the stern layer of SDS micelles that was negatively charged, the surface charge of TMB_{ox2}^{2+} would be deduced. In this case, to simplify the system, TMB_{ox2}^{+} was selected to represent TMB_{ox2} on the stern layer of SDS micelles in aqueous solution. As control, TMB_{ox2} in neutralized state without any protonation, denoted as TMB_{ox2}^{0}, was also explored. The top view and side view of these molecules are shown in Figure S12. It was found that when TMB_{ox2} were coupled with TMB, the positive charge that is indicate as red color in Figure 4, would be re-distributed throughout the entire confused complex, thereby reducing the system energy. Notably, the adsorption energy for $TMB+TMB_{ox2}^{2+}$ reached as high as -1.02 eV, indicative a strong π-π stacking interaction (Figure 4a). It well explained in the free diffusion state TMB was very likely coupled

to TMB_{ox2}, forming a blue confused complex. In contrast, the adsorption energy of TMB+TMB^{+}_{ox2} was -0.77 eV, which was ca. 25% lower than that of the TMB+TMB^{2+}_{ox2} (Figure 4b). It indicated that in the presence of SDS micelles, owing to a decrease in positive charge density around TMB_{ox2} on the stern layer, the coupling of TMB and TMB_{ox2} would be greatly depressed. When the surface positive charge further decreased to zero, i.e., for TMB^{0}_{ox2}, the adsorption energy after π-π stacking was even lower (-0.71 eV). Therefore, in view of the theoretic calculation, the stabilization of TMB_{ox2} on the stern layer reduced the surface positive charge, hampering the formation of an electron transfer complex with TMB.

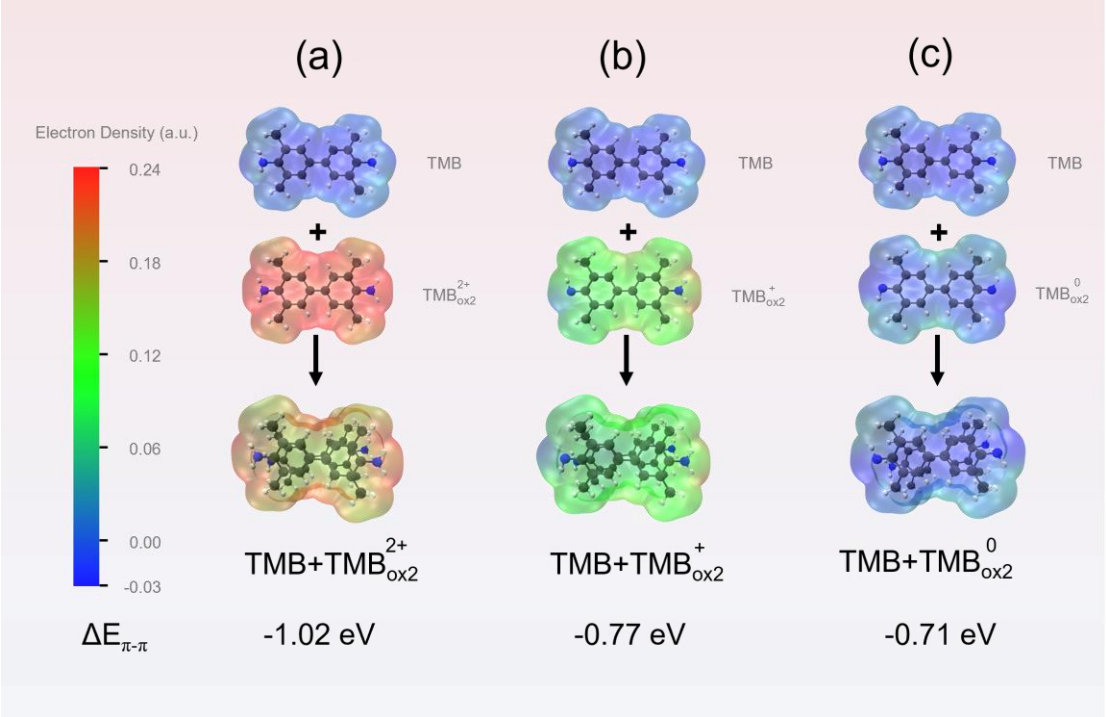

Figure 4. π-π adsorption energy of TMB-based confused complexes. (a) TMB+ TMB^{2+}_{ox2}, (b) TMB+ TMB^{+}_{ox2}, and (c) TMB+ TMB^{0}_{ox2}. The isosurfaces are calculated molecular electrostatic potentials at the 0.001 electron $Bohr^{-3}$. The color scales range from blue (-0.03 a.u.) to red (0.24 a.u.) for all molecules.

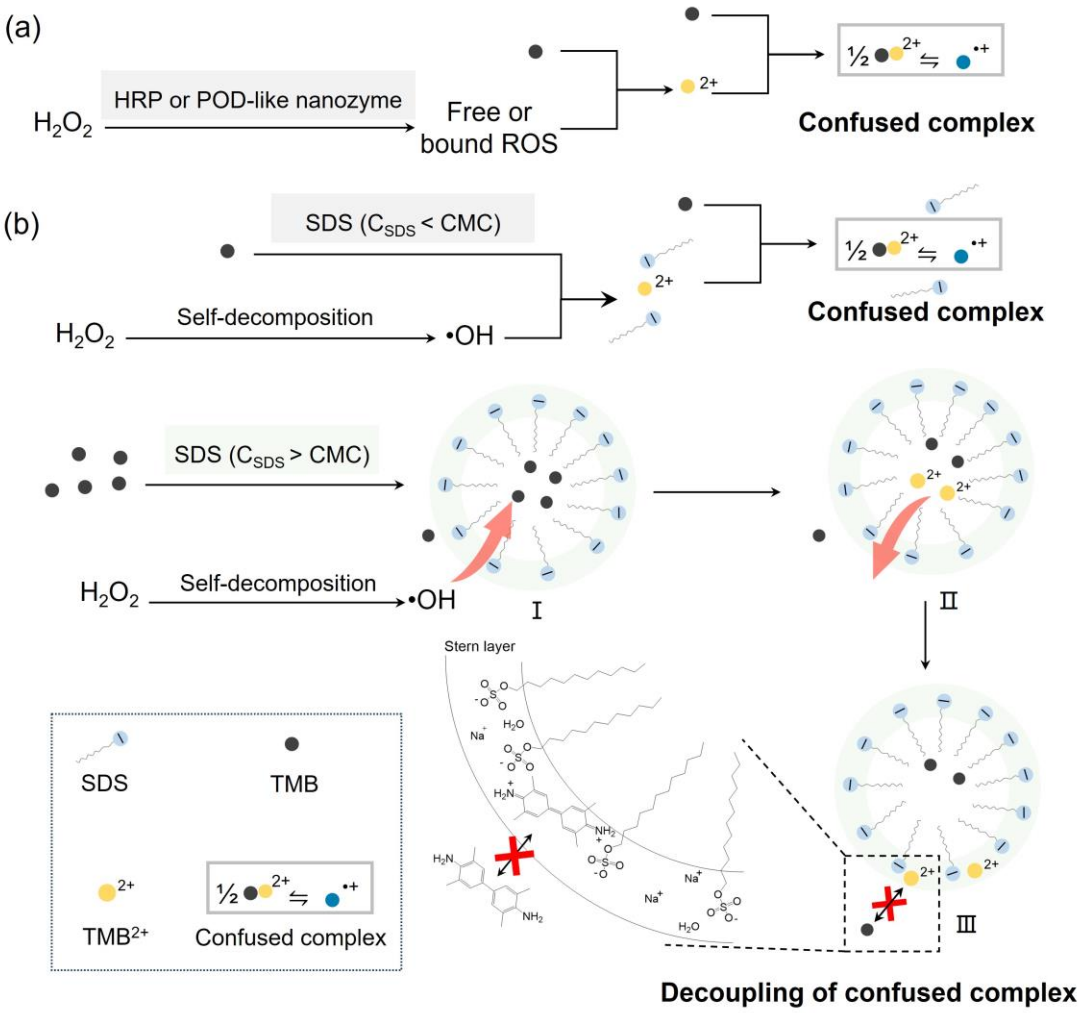

Figure 5. Mechanism of selective two-electron oxidation of TMB via spatial and electrostatic decoupling of confused complex. Reaction pathways of TMB oxidation with H_2O_2 in the presence of natural HRP, POD-like nanozymes (a), and SDS of concentration less (b) and higher (c) than CMC.

Proposed mechanism of selective two-electron oxidation of TMB with SDS micelles. As well known, HRP and conventional POD-like nanozymes generally catalyze the one-electron oxidation of TMB via free or bound ROS pathways (Figure 5a). In contrast, the selective two-electron oxidation pathway for TMB by SDS micelles underwent a different manner. According to the above results, we propose a possible mechanism for TMB oxidation with H_2O_2 in the SDS micelles system. Hydroxyl radicals, generated from the auto-decomposition of hydrogen peroxide under acidic conditions (pH 3.5), were presumably the main source of oxidizing substances. As

shown in Equations 1–4, the TMB oxidation reaction was in equilibrium with the one-electron oxidation products TMB_{ox1} ($TMB^{\bullet+}$ and charge transfer complexes) and two-electron oxidation products TMB_{ox2} (TMB^{2+}).[29, 32] When the concentration of SDS did not reach the CMC, the surfactant chain stabilized the product cations by electrostatic gravitation to promote Equation 2 to the left (Figure 5b). Because the TMB substrate and the product TMB^{2+} were maintained in the same solution phase, an electron transfer complex (TMB-TMB^{2+}) was formed (Equation 3). Equation 4 maintained equilibrium and the practical oxidation product was $TMB^{\bullet+}$ and charge-transfer complexes, which demonstrated the typical blue color. When the SDS concentration exceeded the CMC, a micelle structure was formed. The entire reaction process was confined by micelles, owing to the formation of micellar nanoreactors (Figure 5b, I). The hydrophobic TMB was encapsulated in the hydrophobic cavity. After oxidation with hydroxyl radicals, the hydrophilic products (TMB^{2+}) were transferred to the outer negatively charged stern layer of SDS micelles and adsorbed on it, due to electrostatic interactions (Figure 5b, II). In this case, TMB and TMB^{2+} could not interact to form an electron transfer complex (TMB-TMB^{2+}, Figure 5b, III). In addition, after adsorption on the stern layer of SDS micelles, TMB_{ox2} demonstrated a depressed positive charge and subsequently, also weakened the complexation interaction with TMB. Therefore, SDS micelles not only confined TMB in a hydrophobic microenvironment with accelerated oxidation rate but also decoupled the confused complexation between TMB and TMB_{ox2} that reversed to the conventional one-electron oxidation products TMB_{ox1} via dual ways, i.e., spatial isolation of TMB_{ox2} on the stern layer and electrostatic suppression of the π-π stacking between them. In contrast to the free ROS and bound oxygen intermediate pathways for most peroxidase-like nanozymes in one-electron TMB oxidation, this unique mechanism endowed SDS micelles a selective direct two-electron oxidation pathway. It can be used to address the instability of one-electron oxidation product of TMB as the most widely used chromogenic probe in standard chromogenic bioanalysis.

$$H_2O_2 + H^+ \longrightarrow {}^{\bullet}OH + H_2O \quad (1)$$

$$TMB + {}^{\bullet}OH \longrightarrow TMB^{2+} + H_2O \quad (2)$$

$$TMB^{2+} + TMB \longrightarrow TMB - TMB^{2+} \quad (3)$$

$$TMB - TMB^{2+} \longleftrightarrow 2TMB^{\bullet+} \quad (4)$$

Applications of selective two-electron TMB oxidation for glucose detection with less dependence on measuring time.

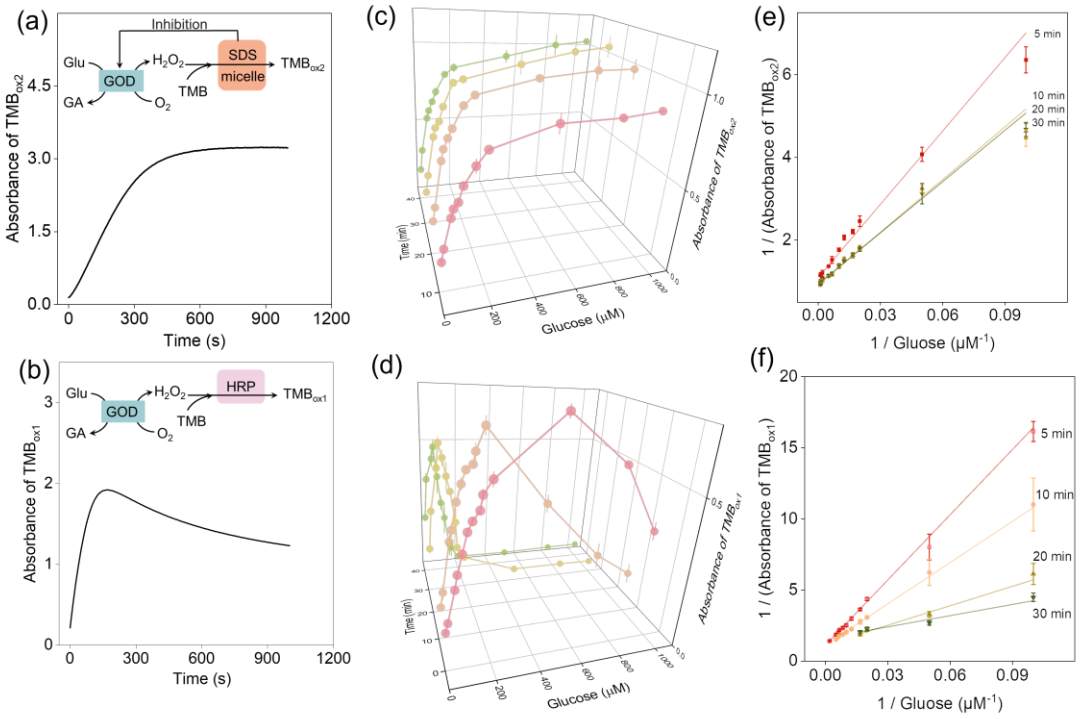

Figure 6. Comparison of SDS and HRP in cascade colorimetric glucose sensors. (a) Time-dependent UV-vis absorption spectra of TMB_{ox2} produced with SDS (20 mM) and in-situ generated H_2O_2 during the biocatalytic oxidation of glucose (100 μM). (b) Time-dependent UV-vis absorption spectra of TMB_{ox1} catalyzed by HRP (5 μg/mL) and in-situ generated H_2O_2 during the biocatalytic oxidation of glucose (100 μM). Glu: glucose, GOD: glucose oxidase, GA: gluconic acid. Plots of absorbance at 450 nm (c, TMB_{ox2}) and 652 nm (d, TMB_{ox1}) versus glucose concentration at different monitoring time (5, 10, 20, 30 min). Double reciprocal plots of the absorbance at 450 nm (e, TMB_{ox2}) and 652 nm (f, TMB_{ox1}) versus glucose concentration at different monitoring time (5, 10, 20, 30 min). Error bars illustrate the standard deviation of three replicate measurements.

Glucose provides much of the basic energy for metabolic processes in living systems

and is an important index in many clinical diseases, such as diabetes, Alzheimers, and cardiovascular disease.[49] To date, various methods had been developed for the detection of glucose, including the electrochemistry, and fluorescence, and colorimetric methods.[50-52] In comparison to other methods, colorimetric techniques are far easier to implement in practical applications. At present, the common colorimetric sensors usually use the blue TMB_{ox1} as the signal probe in the cascaded glucose oxidase (GOD) and HRP (or POD-like enzymes) sensing system. As mentioned earlier, this method suffers from unstable color development. Thus, the highly selective two-electron oxidation pathway of TMB by SDS micelles is highly envisioned to address this long-term challenge. The feasibility of the cascade system (GOD/SDS micelles) for stable glucose sensing was first verified (Figure 6a, see Figure S16 and more details in supporting information). It was observed that SDS micelles can not only be successfully used to construct a cascade system, but also achieve a stable absorbance over a long period of time after a rapid initial linear growth (Figure 6a). As a control, a cascade catalytic system based on GOD and HRP was also measured, in which, H_2O_2 was unceasingly produced, driven by glucose oxidase. It made the product of the HRP-catalyzed oxidation of TMB changed with time, leading to an instable absorbance (Figure 6b). In addition, SDS was also an inhibitor for GOD in the glucose oxidation reaction and had no peroxide suicide inactivation effect of HRP.[53-55] In this sense, the first step of the cascaded reactions (Figure S17) would be simultaneously terminated when the second step initiated, and a broader concentration of H_2O_2 could be tolerated (Figure S18-19). Therefore, compared to HRP, SDS micelles demonstrated excellent stability of absorbance in the cascaded reactions without interferences from the continuation of the former reaction.

Under optimal conditions (Figure S20), the absorbance of oxidized TMB at 450 nm (TMB_{ox2}) increased with glucose concentration varying from 10 to 1000 μM (Figure 6c). The nonlinear calibration curve (Figure 6c) followed the Michaelis-Menten mechanism,[56] reaching a steady state in about 10 min. The reciprocal of the absorbance of TMB_{ox2} obtained by oxidation and the reciprocal of the corresponding glucose

concentration could also fit a similar linear relationship (Figure 6e). The calculated limit of detection (LOD) of glucose was measured to be 1.74 μM at S/N = 3, which was lower than the glucose threshold value diagnosed as diabetes mellitus and comparable or even superior to those of the reported results (Table S1). In contrast, for the enzyme cascade system based on GOD and HRP, the absorbance of TMB_{ox1} increased sharply in the first 2 min and then decreased rapidly with time (Figure 6b). The detection range of the GOD/HRP cascade system also decreased with the increase of time, e.g., significantly narrowing to 10-60 μM after 10 min (Figure 6d and 6f), indicating the instability of the signal output. Such strong dependence of the absorbance of TMB_{ox1} on time would challenge the reliable measurement in practical applications, which generally requires a very precise time control in the experimental operation. Therefore, compared with the GOD/HRP system, the GOD/SDS micelles system was superior in not only detection limit and detection range but also reliability.

To evaluate the practical applicability of SDS micelles in chromogenic biosensing, the detection of glucose in human serum was further explored. A high recovery rate for glucose detection in diluted human serum (10, 30, and 100 μM) was obtained (Table S2), suggesting its practicability for real sample detection. The selectivity of the established glucose detection system was verified using xylose, trehalose, sucrose, fructose, and galactose as interfering substances. As shown in Figure S21, the detection system was capable of resisting other sugar interferences, demonstrating a good selectivity for glucose detection.

Conclusion

In summary, we have demonstrated the effect of sodium dodecyl sulfate (SDS) assemblies on the oxidation pathway of TMB via spatial and electrostatic decoupling of confused complex. Detailed mechanism investigations disclose that a precise two-electron oxidation of TMB is viable in contrast to contrast to the free ROS and bound oxygen intermediate pathways, whereas the presence of spatial and electrostatic decoupling of confused complex can play a decisive role for the selective two-electron oxidation of TMB. As a proof-of-concept application, the special catalytic mechanism

and the uniqueness of the two-electron product made SDS assemblies successfully applied to enhance the reliability of chromogenic bioassay of glucose. Compared to conventional natural enzyme systems (HRP and GOD), SDS assemblies can directly obtain stable two electron product TMB_{ox2} without a terminator. Therefore, the assembly system avoided the disadvantage of signal instability in natural enzyme systems (HRP and GOD) and achieved reliable and sensitive glucose detection in a long period of time. Besides, SDS assemblies was successfully applied to wider concentration H_2O_2 detection (0.1 μM-100 mM). We believe that this approach can not only further advance the development of sensors with stable signal output, but also expand the applications of micelles in the new fields.

Acknowledgements

This work was supported by the National Natural Science Foundation of China (22174014 and 22074015).

References

1. Yang, J., Good Timing for Precision Chemistry. *Precis. Chem.* **2023,** *1*, 1-2.

2. Migliorini, F.; Monciatti, E.; Romagnoli, G.; Parisi, M. L.; Taubert, J.; Vogt, M.; Langer, R.; Petricci, E., Switching Mechanistic Pathways by Micellar Catalysis: A Highly Selective Rhodium Catalyst for the Hydroaminomethylation of Olefins with Anilines in Water. *ACS Catal.* **2023,** *13*, 2702-2714.

3. Holland, V. R.; Saunders, B. C.; Rose, F. L.; Walpole, A. L., A safer substitute for benzidine in the detection of blood. *Tetrahedron* **1974,** *30*, 3299-3302.

4. Zhang, X.; Yang, Q.; Lang, Y.; Jiang, X.; Wu, P., Rationale of 3,3′,5,5′-Tetramethylbenzidine as the Chromogenic Substrate in Colorimetric Analysis. *Anal. Chem.* **2020,** *92*, 12400-12406.

5. Fu, Y.; Du, C.; Zhang, Q.; Xiao, K.; Zhang, X.; Chen, J., Colorimetric and Photocurrent-Polarity-Switching Photoelectrochemical Dual-Mode Sensing Platform for Highly Selective Detection of Mercury Ions Based on the Split G-Quadruplex–

Hemin Complex. *Anal. Chem.* **2022,** *94*, 15040-15047.

6. Yang, S.; Jia, W. Z.; Qian, Q. Y.; Zhou, Y. G.; Xia, X. H., Simple Approach for Efficient Encapsulation of Enzyme in Silica Matrix with Retained Bioactivity. *Anal. Chem.* **2009,** *81*, 3478-3484.

7. Zhu, Y.; Xu, Y.; Xue, Y.; Fan, G.; Zhang, P.; Zhao, W.; Xu, J.; Chen, H., Three-Dimensional CdS@Carbon Fiber Networks: Innovative Synthesis and Application as a General Platform for Photoelectrochemical Bioanalysis. *Anal. Chem.* **2019,** *91*, 6419-6423.

8. Li, X.; Du, Y.; Wang, H.; Ma, H.; Wu, D.; Ren, X.; Wei, Q.; Xu, J., Self-Supply of H_2O_2 and O_2 by Hydrolyzing CaO_2 to Enhance the Electrochemiluminescence of Luminol Based on a Closed Bipolar Electrode. *Anal. Chem.* **2020,** *92*, 12693-12699.

9. Chen, C.; Zhao, D.; Sun, J.; Yang, X., Colorimetric Logic Gate for Pyrophosphate and Pyrophosphatase via Regulating the Catalytic Capability of Horseradish Peroxidase. *ACS Appl. Mater. Interfaces* **2016,** *8*, 29529-29535.

10. Fu, G.; Sanjay, S. T.; Zhou, W.; Brekken, R. A.; Kirken, R. A.; Li, X., Exploration of Nanoparticle-Mediated Photothermal Effect of TMB-H2O2 Colorimetric System and Its Application in a Visual Quantitative Photothermal Immunoassay. *Anal. Chem.* **2018,** *90*, 5930-5937.

11. Huang, J.; Jiao, L.; Xu, W.; Fang, Q.; Wang, H.; Cai, X.; Yan, H.; Gu, W.; Zhu, C., Immobilizing Enzymes on Noble Metal Hydrogel Nanozymes with Synergistically Enhanced Peroxidase Activity for Ultrasensitive Immunoassays by Cascade Signal Amplification. *ACS Appl. Mater. Interfaces* **2021,** *13*, 33383-33391.

12. Josephy, P. D.; Eling, T.; Mason, R. P., The horseradish peroxidase-catalyzed oxidation of 3,5,3',5'-tetramethylbenzidine. Free radical and charge-transfer complex intermediates. *J. Biol. Chem.* **1982,** *257*, 3669-3675.

13. Lathwal, S.; Sikes, H. D., Assessment of colorimetric amplification methods in a paper-based immunoassay for diagnosis of malaria. *Lab Chip* **2016,** *16*, 1374-1382.

14. Vazquez-Alvarado, M.; Vanasupa, S.; Valdez, E. H.; Pama, A. M.; Crowder, M. J.; Vanasupa, L.; Martinez, N. W.; Martinez, A. W., Evaluation of chromogenic

substrates for horseradish peroxidase on paper-based microfluidic devices. *Sens. Actuators, B* **2023,** *377*, 133028.

15. Zhang, Y.; Zhang, B.; Ye, X.; Yan, Y.; Huang, L.; Jiang, Z.; Tan, S.; Cai, X., Electrochemical immunosensor for interferon-γ based on disposable ITO detector and HRP-antibody-conjugated nano gold as signal tag. *Materials Science and Engineering: C* **2016,** *59*, 577-584.

16. Sun, L.-P.; Huang, Y.; Huang, T.; Yuan, Z.; Lin, W.; Sun, Z.; Yang, M.; Xiao, P.; Ma, J.; Wang, W., Optical microfiber reader for enzyme-linked immunosorbent assay. *Anal. Chem.* **2019,** *91*, 14141-14148.

17. Wu, S.; Sun, Z.; Peng, Y.; Han, Y.; Li, J.; Zhu, S.; Yin, Y.; Li, G., Peptide-functionalized metal-organic framework nanocomposite for ultrasensitive detection of secreted protein acidic and rich in cysteine with practical application. *Biosens. Bioelectron.* **2020,** *169*, 112613.

18. Gao, L.; Zhuang, J.; Nie, L.; Zhang, J.; Zhang, Y.; Gu, N.; Wang, T.; Feng, J.; Yang, D.; Perrett, S.; Yan, X., Intrinsic peroxidase-like activity of ferromagnetic nanoparticles. *Nat. Nanotechnol.* **2007,** *2*, 577-583.

19. Ji, S.; Jiang, B.; Hao, H.; Chen, Y.; Dong, J.; Mao, Y.; Zhang, Z.; Gao, R.; Chen, W.; Zhang, R.; Liang, Q.; Li, H.; Liu, S.; Wang, Y.; Zhang, Q.; Gu, L.; Duan, D.; Liang, M.; Wang, D.; Yan, X.; Li, Y., Matching the kinetics of natural enzymes with a single-atom iron nanozyme. *Nat. Catal.* **2021,** *4*, 407-417.

20. Ma, C. B.; Xu, Y.; Wu, L.; Wang, Q.; Zheng, J.; Ren, G.; Wang, X.; Gao, X.; Zhou, M.; Wang, M.; Wei, H., Guided Synthesis of a Mo/Zn Dual Single‐Atom Nanozyme with Synergistic Effect and Peroxidase‐like Activity. *Angew. Chem. Int. Ed.* **2022,** *61*, e202116170.

21. Ruan, X.; Liu, D.; Niu, X.; Wang, Y.; Simpson, C. D.; Cheng, N.; Du, D.; Lin, Y., 2D Graphene Oxide/Fe-MOF Nanozyme Nest with Superior Peroxidase-Like Activity and Its Application for Detection of Woodsmoke Exposure Biomarker. *Anal. Chem.* **2019,** *91*, 13847-13854.

22. Hu, W.; Younis, M. R.; Zhou, Y.; Wang, C.; Xia, X., In situ fabrication of

ultrasmall gold nanoparticles/2D MOFs hybrid as nanozyme for antibacterial therapy. *Small* **2020,** *16*, 2000553.

23. Zhen, W.; Liu, Y.; Wang, W.; Zhang, M.; Hu, W.; Jia, X.; Wang, C.; Jiang, X., Specific "Unlocking" of a Nanozyme - Based Butterfly Effect To Break the Evolutionary Fitness of Chaotic Tumors. *Angew. Chem. Int. Ed.* **2020,** *59*, 9491-9497.

24. Yu, L.; Chang, J.; Zhuang, X.; Li, H.; Hou, T.; Li, F., Two-Dimensional Cobalt-Doped Ti_3C_2 MXene Nanozyme-Mediated Homogeneous Electrochemical Strategy for Pesticides Assay Based on In Situ Generation of Electroactive Substances. *Anal. Chem.* **2022,** *94*, 3669-3676.

25. Mikuka, P.; Veea, Z., Effect of complexones and tensides on selectivity of nitrogen dioxide determination in air with a chemiluminescence aerosol detector. *Anal. Chim. Acta* **2000,** *410*, 159-165.

26. La Sorella, G.; Strukul, G.; Scarso, A., Recent advances in catalysis in micellar media. *Green Chem.* **2015,** *17*, 644-683.

27. Li, M.; Su, H.; Tu, Y.; Shang, Y.; Liu, Y.; Peng, C.; Liu, H., Development and Application of an Efficient Medium for Chromogenic Catalysis of Tetramethylbenzidine with Horseradish Peroxidase. *ACS Omega* **2019,** *4*, 5459-5470.

28. Banerjee, M.; Panjikar, P. C.; Bhutia, Z. T.; Bhosle, A. A.; Chatterjee, A., Micellar nanoreactors for organic transformations with a focus on "dehydration" reactions in water: A decade update. *Tetrahedron* **2021,** *88*, 132142.

29. Josephy, P. D.; Mason, R. P.; Eling, T., Cooxidation of the clinical reagent 3, 5, 3′ 5′-tetramethylbenzidine by prostaglandin synthase. *Cancer Res.* **1982,** *42*, 2567-2570.

30. Imberty, A.; Goldberg, R.; Catesson, A.-M., Tetramethylbenzidine and p-phenylenediamine-pyrocatechol for peroxidase histochemistry and biochemistry: two new, non-carcinogenic chromogens for investigating lignification process. *Plant Sci. Lett.* **1984,** *35*, 103-108.

31. Verlander, C., *Detection of horseradish peroxidase by colorimetry*. 1992; p 185-201.

32. Misono, Y.; Ohkata, Y.; Morikawa, T.; Itoh, K., Resonance Raman and absorption spectroscopic studies on the electrochemical oxidation processes of 3, 3′, 5, 5′-tetramethylbenzidine. *J. Electroanal. Chem.* **1997,** *436*, 203-212.

33. Sobhani, S.; Vafaee, A., Micellar solution of sodium dodecyl sulfate (SDS) catalyzes Kabacknik-Fields reaction in aqueous media. *Synthesis* **2009,** *2009*, 1909-1915.

34. Frias Batista, L. M.; Meader, V. K.; Romero, K.; Kunzler, K.; Kabir, F.; Bullock, A.; Tibbetts, K. M., Kinetic Control of $[AuCl_4]^-$ Photochemical Reduction and Gold Nanoparticle Size with Hydroxyl Radical Scavengers. *J. Phys. Chem. B* **2019,** *123*, 7204-7213.

35. Gao, L.; Zhuang, J.; Nie, L.; Zhang, J.; Zhang, Y.; Gu, N.; Wang, T.; Feng, J.; Yang, D.; Perrett, S.; Yan, X., Intrinsic peroxidase-like activity of ferromagnetic nanoparticles. *Nat. Nanotechnol.* **2007,** *2*, 577-583.

36. Jiao, L.; Wu, J.; Zhong, H.; Zhang, Y.; Xu, W.; Wu, Y.; Chen, Y.; Yan, H.; Zhang, Q.; Gu, W.; Gu, L.; Beckman, S. P.; Huang, L.; Zhu, C., Densely Isolated FeN_4 Sites for Peroxidase Mimicking. *ACS Catal.* **2020,** *10*, 6422-6429.

37. Kunitake, T.; Shinkai, S., Catalysis by micelles, membranes and other aqueous aggregates as models of enzyme action. *Adv. Phys. Org. Chem.* **1980,** *17*, 435-487.

38. Zhou, Q.; When, Z., Research on micellar catalysis and micellar mimetic enzymes. *Chem. Bull.* **1987,** *5*, 21-26.

39. Hassan, P.; Raghavan, S. R.; Kaler, E. W., Microstructural changes in SDS micelles induced by hydrotropic salt. *Langmuir* **2002,** *18*, 2543-2548.

40. Schäfer, K.; Kolli, H. B.; Killingmoe Christensen, M.; Bore, S. L.; Diezemann, G.; Gauss, J.; Milano, G.; Lund, R.; Cascella, M., Supramolecular Packing Drives Morphological Transitions of Charged Surfactant Micelles. *Angew. Chem. Int. Ed.* **2020,** *59*, 18591-18598.

41. Zana, R.; Kaler, E. W., *Giant micelles: properties and applications*. CRC press: 2007; Vol. 140.

42. Jensen, G. V.; Lund, R.; Gummel, J.; Narayanan, T.; Pedersen, J. S.,

Monitoring the Transition from Spherical to Polymer-like Surfactant Micelles Using Small-Angle X-Ray Scattering. *Angew. Chem. Int. Ed.* **2014,** *53*, 11524-11528.

43. Paleologos, E. K.; Vlessidis, A. G.; Karayannis, M. I.; Evmiridis, N. P., On-line sorption preconcentration of metals based on mixed micelle cloud point extraction prior to their determination with micellar chemiluminescence. *Anal. Chim. Acta* **2003,** *477*, 223-231.

44. Zhao, D.; Zhang, G.; Jiang, T.; Deng, Z.; Wu, Y., Flow-injection chemiluminescence method for determination of critical micelle concentration of surfactants. *Int. J. Environ. Anal. Chem.* **2015,** *95*, 980-988.

45. Danov, K. D.; Kralchevsky, P. A.; Stoyanov, S. D.; Cook, J. L.; Stott, I. P., Analytical modeling of micelle growth. 1. Chain-conformation free energy of binary mixed spherical, wormlike and lamellar micelles. *J. Colloid Interface Sci.* **2019,** *547*, 245-255.

46. Ji, W. X.; Yan, J. J.; Chen, E. Q.; Li, Z. C.; Liang, D. H., In situ and online monitoring polymerization-induced micellization. *Macromolecules* **2008,** *41*, 4914-4919.

47. Nowick, J. S.; Chen, J. S.; Noronha, G., Molecular recognition in micelles: the roles of hydrogen bonding and hydrophobicity in adenine-thymine base-pairing in SDS micelles. *J. Am. Chem. Soc.* **1993,** *115*, 7636-7644.

48. Suratkar, V.; Mahapatra, S., Solubilization Site of Organic Perfume Molecules in Sodium Dodecyl Sulfate Micelles: New Insights from Proton NMR Studies. *J. Colloid Interface Sci.* **2000,** *225*, 32-38.

49. Cohain, A. T.; Barrington, W. T.; Jordan, D. M.; Beckmann, N. D.; Argmann, C. A.; Houten, S. M.; Charney, A. W.; Ermel, R.; Sukhavasi, K.; Franzen, O., An integrative multiomic network model links lipid metabolism to glucose regulation in coronary artery disease. *Nat. Commun.* **2021,** *12*, 547.

50. Liu, B.; Sun, Z.; Huang, P.-J. J.; Liu, J., Hydrogen Peroxide Displacing DNA from Nanoceria: Mechanism and Detection of Glucose in Serum. *J. Am. Chem. Soc.* **2015,** *137*, 1290-1295.

51. Long, B.; Zhao, Y.; Cao, P.; Wei, W.; Mo, Y.; Liu, J.; Sun, C.-J.; Guo, X.; Shan, C.; Zeng, M.-H., Single-Atom Pt Boosting Electrochemical Nonenzymatic Glucose Sensing on $Ni(OH)_2$/N-Doped Graphene. *Anal. Chem.* **2022,** *94*, 1919-1924.

52. Ma, C. B.; Xu, Y.; Wu, L.; Wang, Q.; Zheng, J. J.; Ren, G.; Wang, X.; Gao, X.; Zhou, M.; Wang, M.; Wei, H., Guided Synthesis of a Mo/Zn Dual Single - Atom Nanozyme with Synergistic Effect and Peroxidase - like Activity. *Angew. Chem. Int. Ed.* **2022,** *61*, e202116170.

53. Lau, F. W.; Bowie, J. U., A Method for Assessing the Stability of a Membrane Protein. *Biochemistry* **1997,** *36*, 5884-5892.

54. Otzen, D., Protein–surfactant interactions: A tale of many states. *Biochim. Biophys. Acta* **2011,** *1814*, 562-591.

55. Bratton, M. R.; Pressler, M. A.; Hosler, J. P., Suicide inactivation of cytochrome c oxidase: catalytic turnover in the absence of subunit III alters the active site. *Biochemistry* **1999,** *38*, 16236-16245.

56. Hong, Q.; Shen, Y.; Liu, S.; Zhang, Y., Re-Examination of Plotting Analytical Response against Different Forms of Concentration. *Anal. Chem.* **2021,** *93*, 11910-11914.